

Supplementary Information

The weekly cycle of photosynthesis in Europe reveals the negative impact of particulate pollution on ecosystem productivity

Liyin He^{1*}, Lorenzo Rosa^{1*}, David B. Lobell^{2,3}, Yuan Wang², Yi Yin^{4,5}, Russell Doughty⁶, Yitong Yao⁴, Joseph A. Berry¹, Christian Frankenberg^{4,7}

¹ Department of Global Ecology, Carnegie Institution for Science, Stanford, CA 94305, USA

² Department of Earth System Science, Stanford University, Stanford, CA 94305, USA

³ Center on Food Security and the Environment, Stanford University, Stanford, CA 94305, USA

⁴ Division of Geological and Planetary Sciences, California Institute of Technology, Pasadena, CA 91125, USA

⁵ Now at the Department of Environmental Studies, New York University, New York, NY 10003, USA

⁶ College of Atmospheric and Geographic Sciences, University of Oklahoma, Norman, OK 73019, USA

⁷ Jet Propulsion Laboratory, California Institute of Technology, Pasadena, CA 91109, USA

***Corresponding author:** lhe@carnegiescience.edu and lrosa@carnegiescience.edu

This PDF file includes:

- Supplementary Text S1
- Supplementary Figures 1 to 22
- Supplementary Table S1 and S2

Supplementary Text S1. Quantifying Potential Increase in Ecosystem Respiration due to Temperature Rise under Reduced Aerosol Conditions

Reduced aerosol pollution can potentially lead to an increase in temperature, thereby enhancing ecosystem respiration. The key question is whether the increase in gross primary productivity (GPP) outweighs the increase in respiration, resulting in an increase in net ecosystem productivity (NEP), or vice versa. We address this question at both the flux tower scale and the continental scale in the following analysis.

At the flux tower scale, we examine the changes in GPP and ecosystem respiration between weekends and weekdays and find that, for most sites, both increase during the weekend. However, the magnitude of the increase in GPP is larger than that of ecosystem respiration, leading to an increase in NEP (see **Supplementary Figure 15**).

At the continental scale, remote sensing techniques can only track GPP and not ecosystem respiration. To approximate the change in ecosystem respiration due to elevated temperature, we use a simplified model. We employ the well-established equation:

$$R(T) = R_{25} \times Q_{10}^{\frac{T-25}{10}}$$

where $R(T)$ represents the ecosystem respiration at a specific temperature T , R_{25} denotes the baseline respiration at the reference temperature of 25°C, and Q_{10} represents the factor by which respiration rate increases for every 10°C rise in temperature.

The ratio of ecosystem respiration between the weekend and weekday is calculated as:

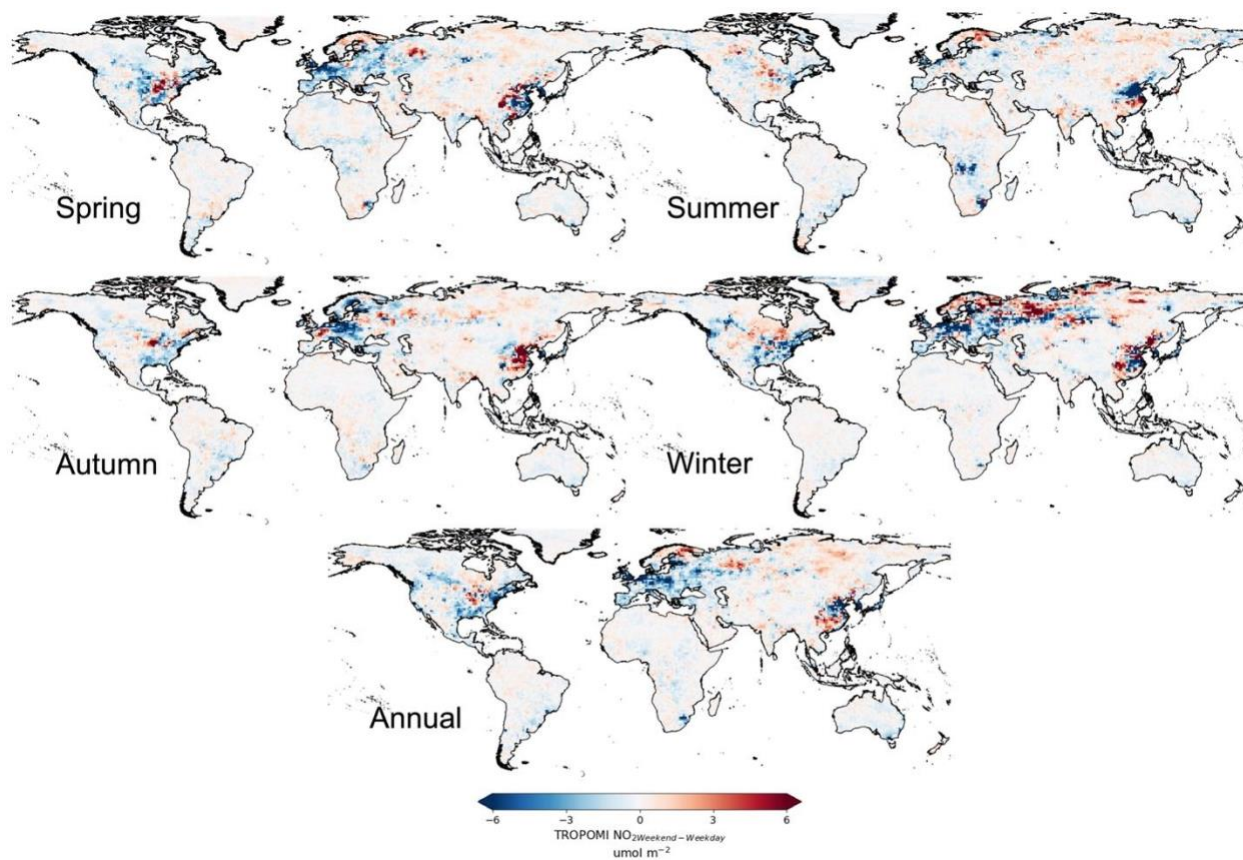
$$\frac{R(T_{weekend})}{R(T_{weekday})} = Q_{10}^{\frac{T_{weekend}-T_{weekday}}{10}}$$

The relative change in ecosystem respiration over the weekend compared to the weekday is computed as:

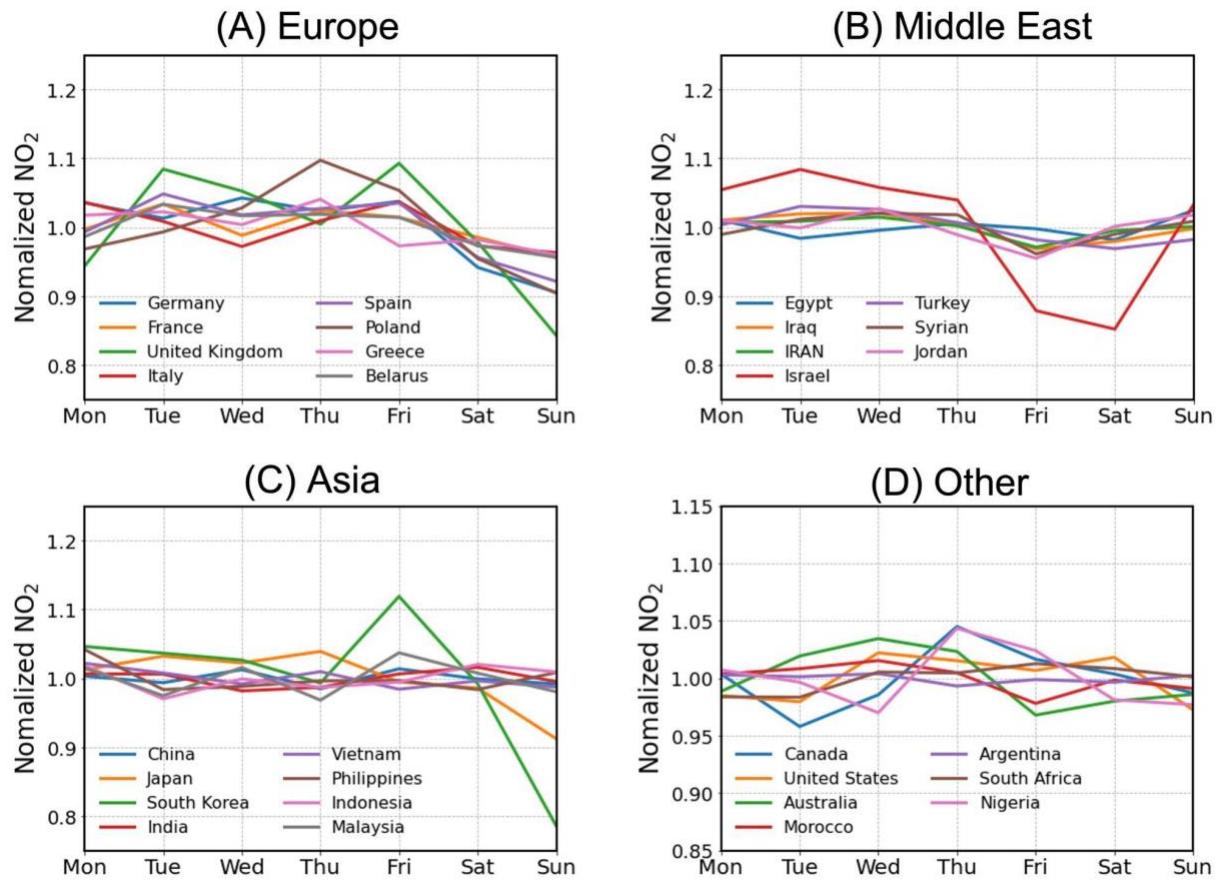
$$\left(\frac{R(T_{weekend})}{R(T_{weekday})} - 1 \right) \times 100\%$$

First, we calculate Q_{10} values using eddy covariance measurements at each flux tower site (**Supplementary Table S1**). The derived Q_{10} values spans from a minimum of 1.0 to a maximum of 3.0. Next, we employed an iterative approach to calculate the relative change in ecosystem respiration over the weekend compared to the weekday. This involved exploring a range of Q_{10} values from 1.0 to 3.0 with a step size of 0.2. The calculations were based on the weekend minus weekday difference in air temperature derived from ERA5 daily air temperature.

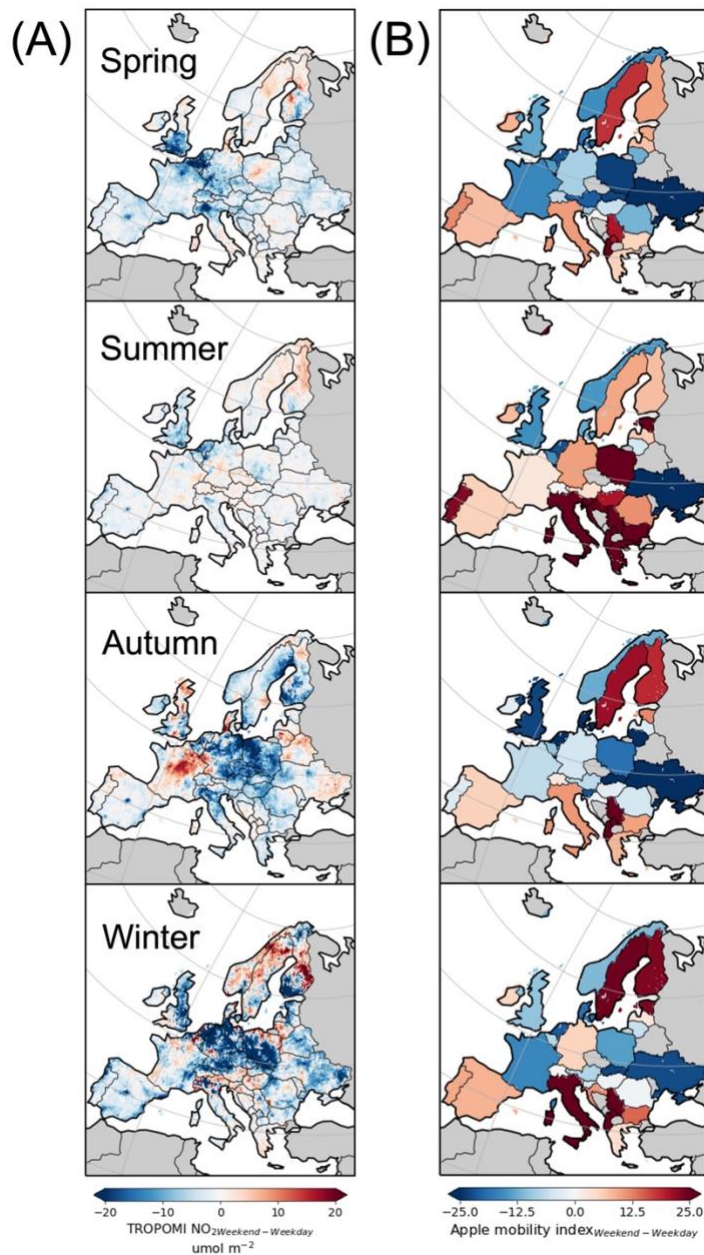
The resulting Europe-averaged relative change in ecosystem respiration over the weekend was plotted for each Q_{10} step (**Supplementary Figure 22**). Notably, the analysis revealed a positive correlation between Q_{10} values and ecosystem respiration. Specifically, when Q_{10} was set at 2, ecosystem respiration increased by 0.2%, and when Q_{10} reached 3, the increase amounted to 0.35%. It is important to note that these observed changes in ecosystem respiration are relatively minor in comparison to the approximately 2.5% increase in SIF (or GPP) observed during the weekend.



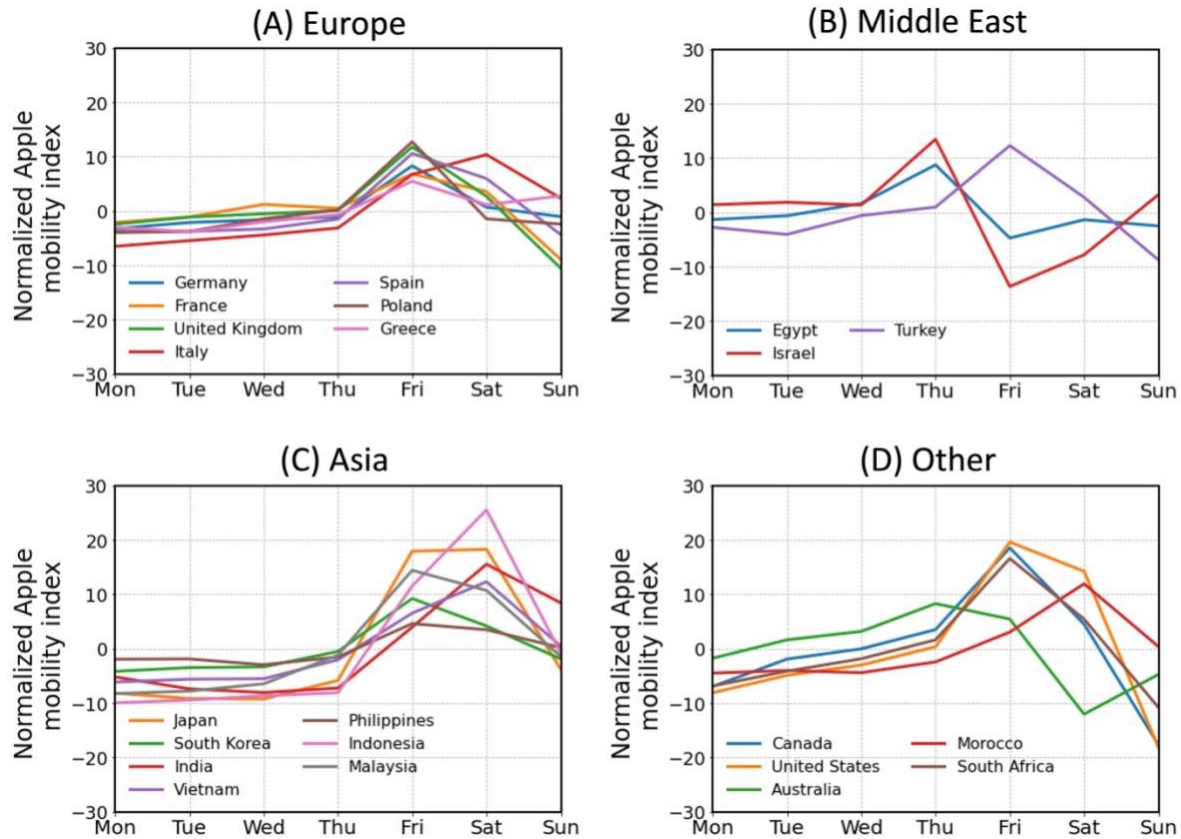
Supplementary Figure 1. Map of global weekend minus weekday TROPOMI NO₂ during 2019, 2020 and 2021. Spring refers to March, April, and May. Summer refers to June, July, and August. Autumn refers to September, October, and November. Winter refers to December, January, and February.



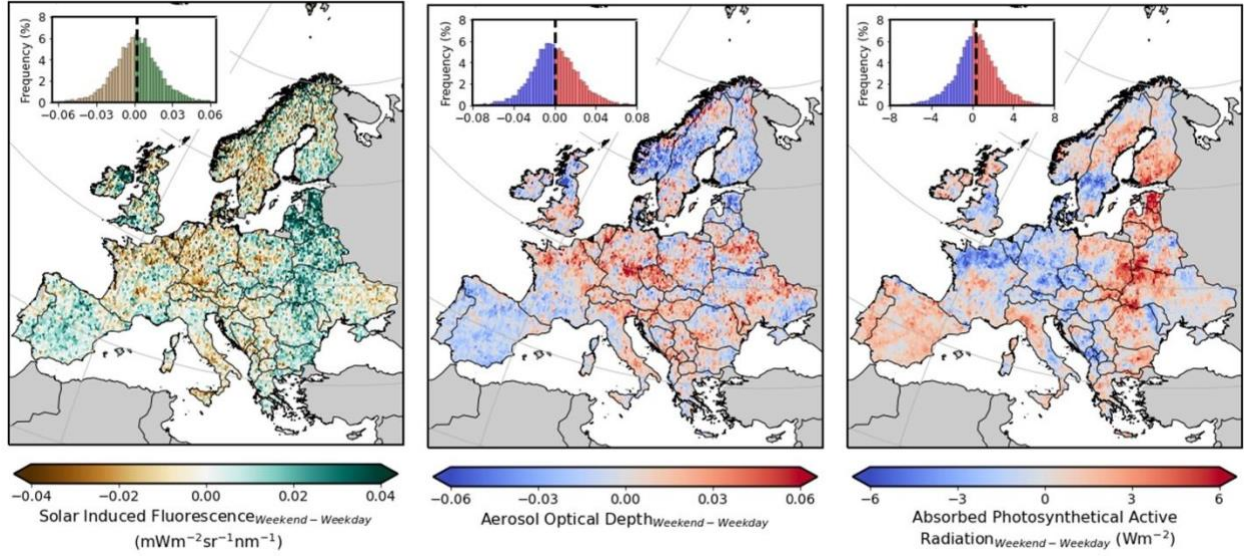
Supplementary Figure 2. Mean normalized TROPOMI NO₂ on different days of the week in typical countries, including (a) Europe, (b) the Middle East, (c) Asia, and (d) countries in the Americas, Africa, and Australia, during 2019, 2020, and 2021. The values have been normalized by dividing them with their corresponding mean values.



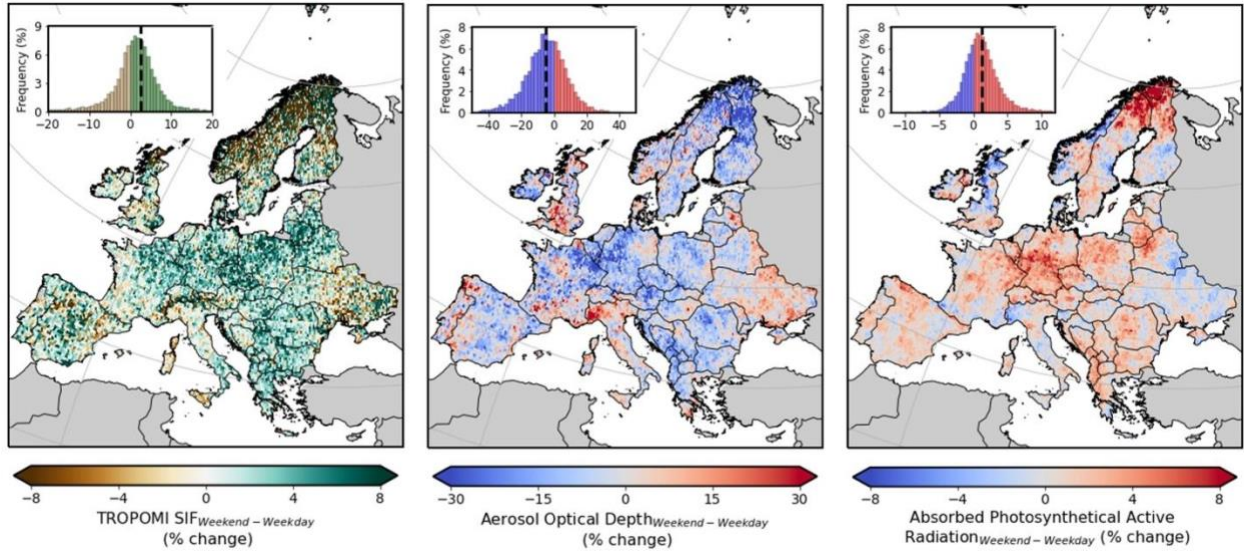
Supplementary Figure 3. Map of weekend minus weekday (A) TROPOMI NO₂ and (B) Apple mobility index (B) in Europe. TROPOMI NO₂ is taken in 2019 and 2021, while the mobility data covers the period from March 2020 to March 2022. Apple mobility index represents the traffic volume on the day compared to a baseline period of January 13th, 2020 and is taken from https://github.com/ActiveConclusion/COVID19_mobility/.



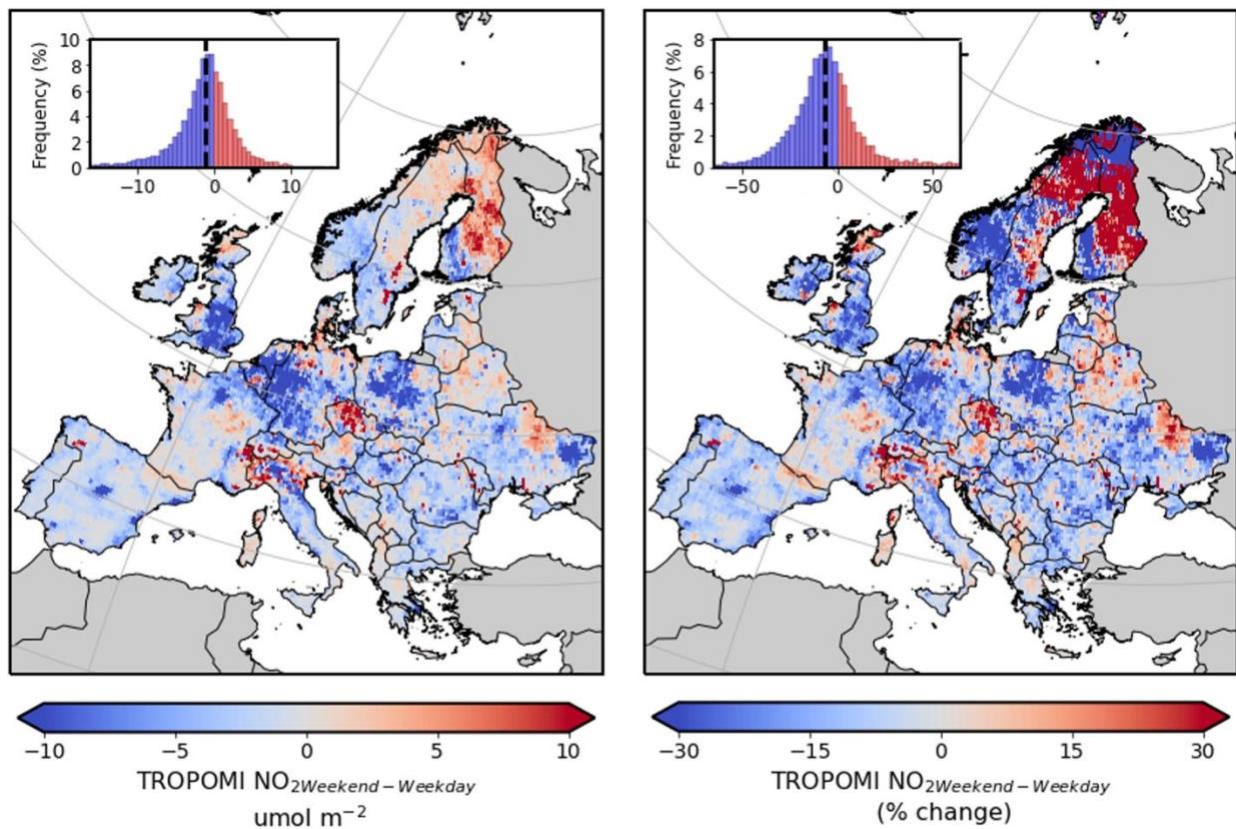
Supplementary Figure 4. Mean normalized Apple mobility index on different days of the week in typical countries, including (a) Europe, (b) the Middle East, (c) Asia, and (d) countries in the Americas, Africa, and Australia, during March 2020 to March 2022. The values have been normalized by dividing them with their corresponding mean values. The data is taken from https://github.com/ActiveConclusion/COVID19_mobility/.



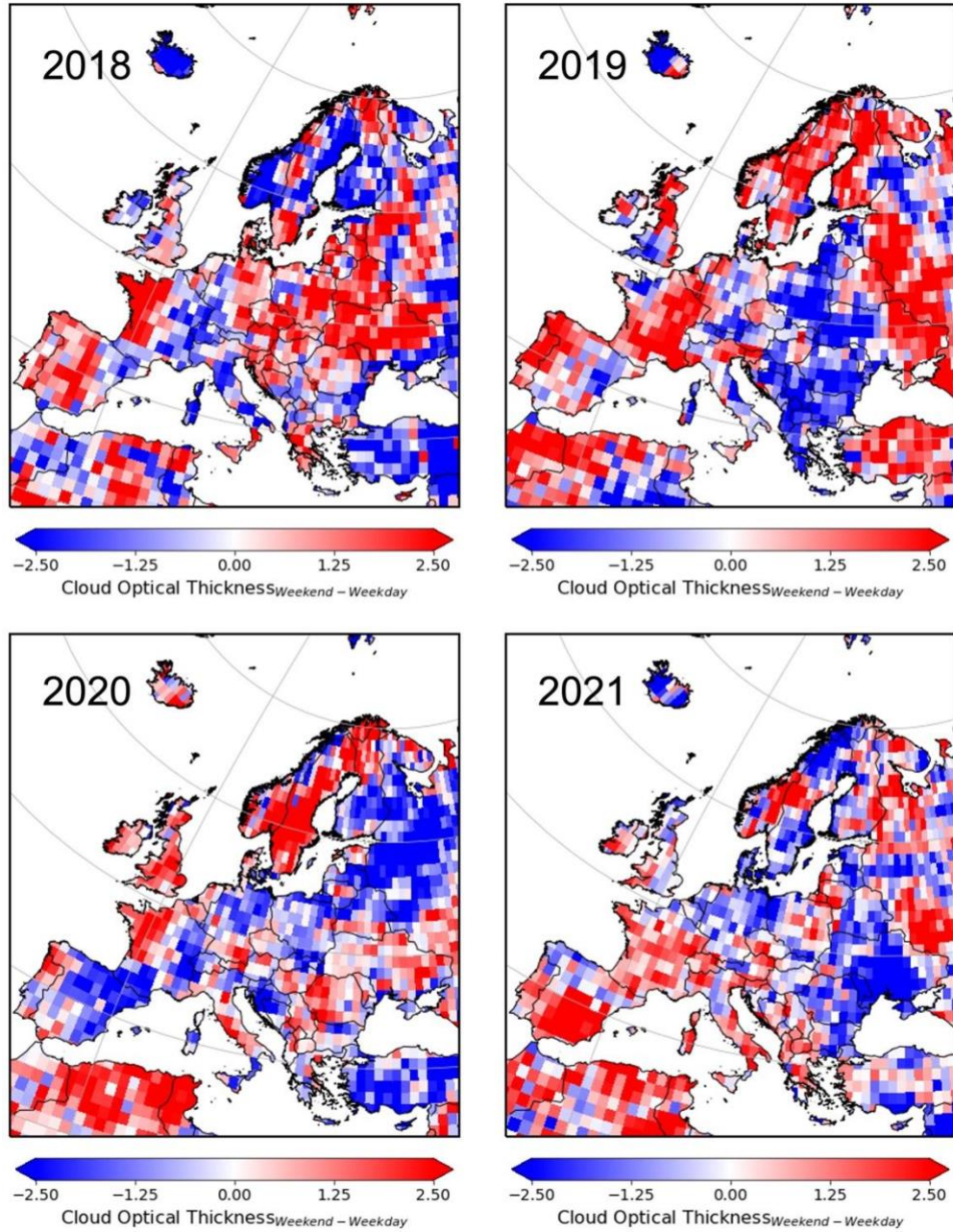
Supplementary Figure 5. The difference of TROPOMI solar induced fluorescence, aerosol optical depth, and absorbed photosynthetic active radiation in Europe during the COVID pandemic (2020) between weekend and weekday. The insert histograms show the distribution of the corresponding variable.



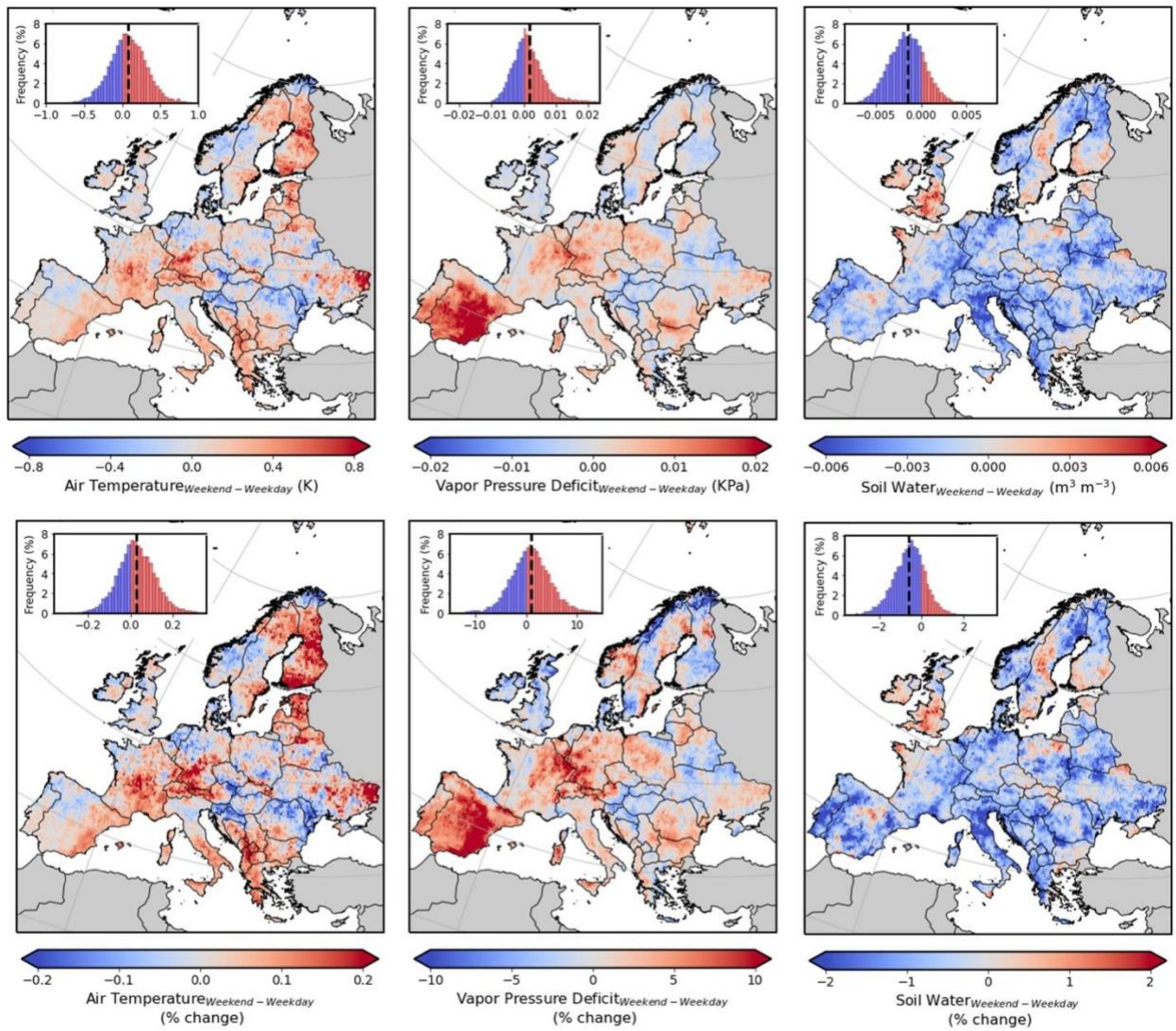
Supplementary Figure 6. Percent changes between weekend and weekday of TROPOMI solar induced fluorescence, aerosol optical depth and absorbed photosynthetic active radiation in Europe during 2018, 2019 and 2021. The insert histograms show the distribution of the corresponding variable, and dashed black lines represent the median values.



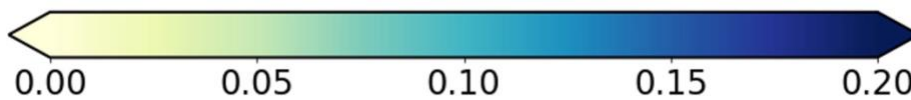
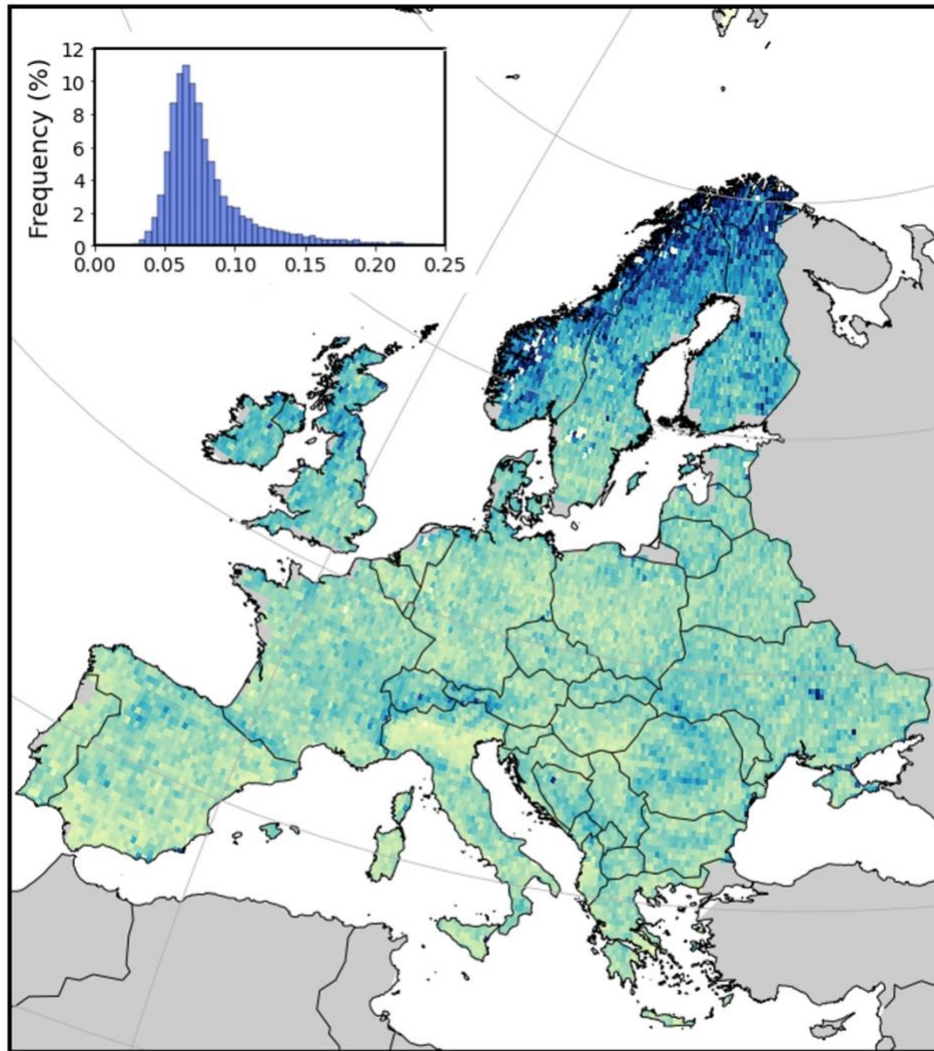
Supplementary Figure 7. Map of weekend minus weekday TROPOMI NO₂ in Europe during 2019 and 2021. The left panel shows the raw values, and the right panel shows the percentage change. The insert histograms illustrate the distribution of the corresponding variable, and dashed black lines represent the median values.



Supplementary Figure 8. Map of the difference in MODIS cloud optical thickness between weekends and weekdays from 2018 to 2021.

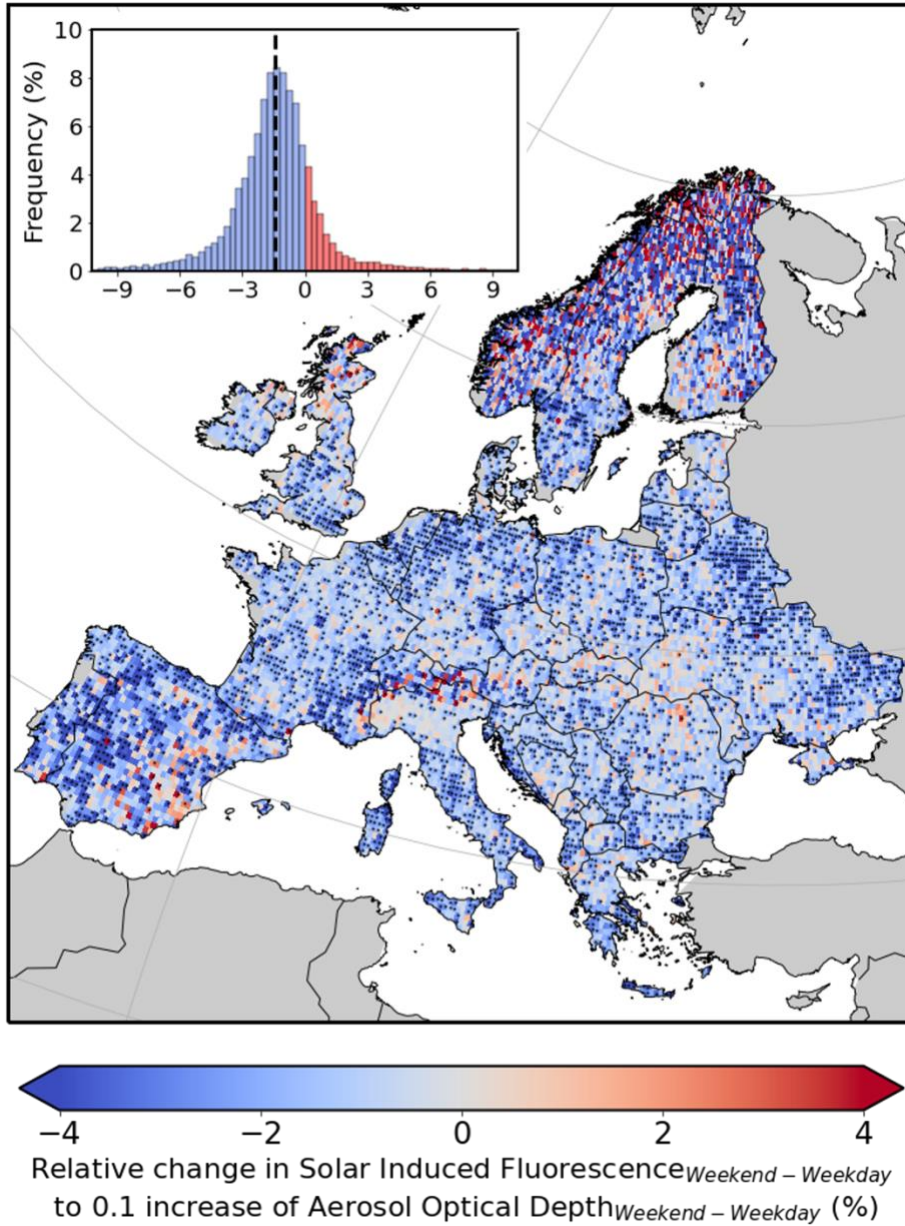


Supplementary Figure 9. The difference of ERA5 air temperature, vapor pressure deficit, and soil moisture between weekend and weekday in Europe during 2018, 2019 and 2021. The top panels display the raw values, and the bottom panels show the percentage change. The insert histograms show the distribution of the corresponding variable, and dashed black lines represent the median values.

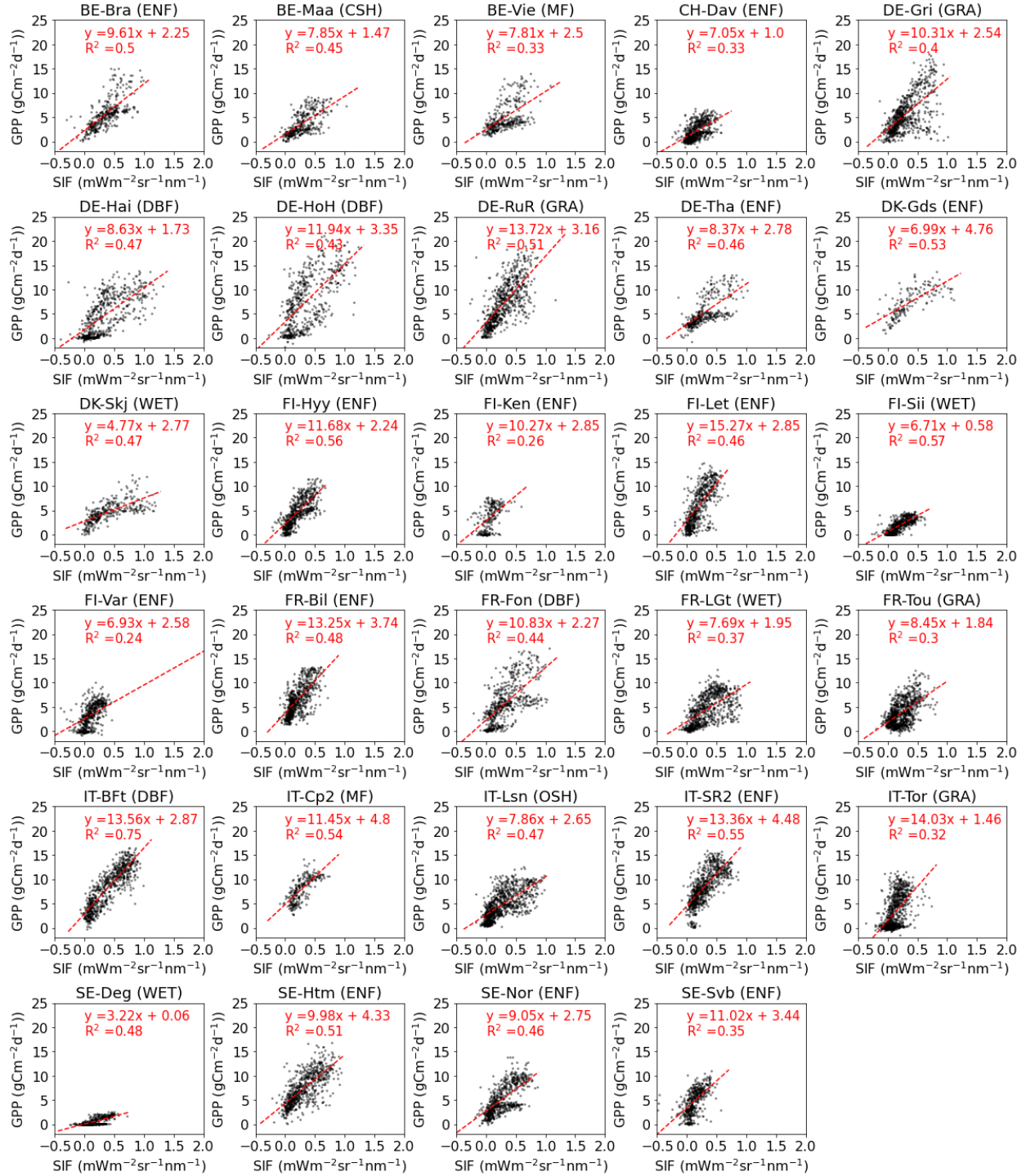


Standard error of sensitivity of Solar Induced Fluorescence_{Weekend – Weekday}
to Aerosol Optical Depth_{Weekend – Weekday} ($\text{mWm}^{-2}\text{sr}^{-1}\text{nm}^{-1}$)

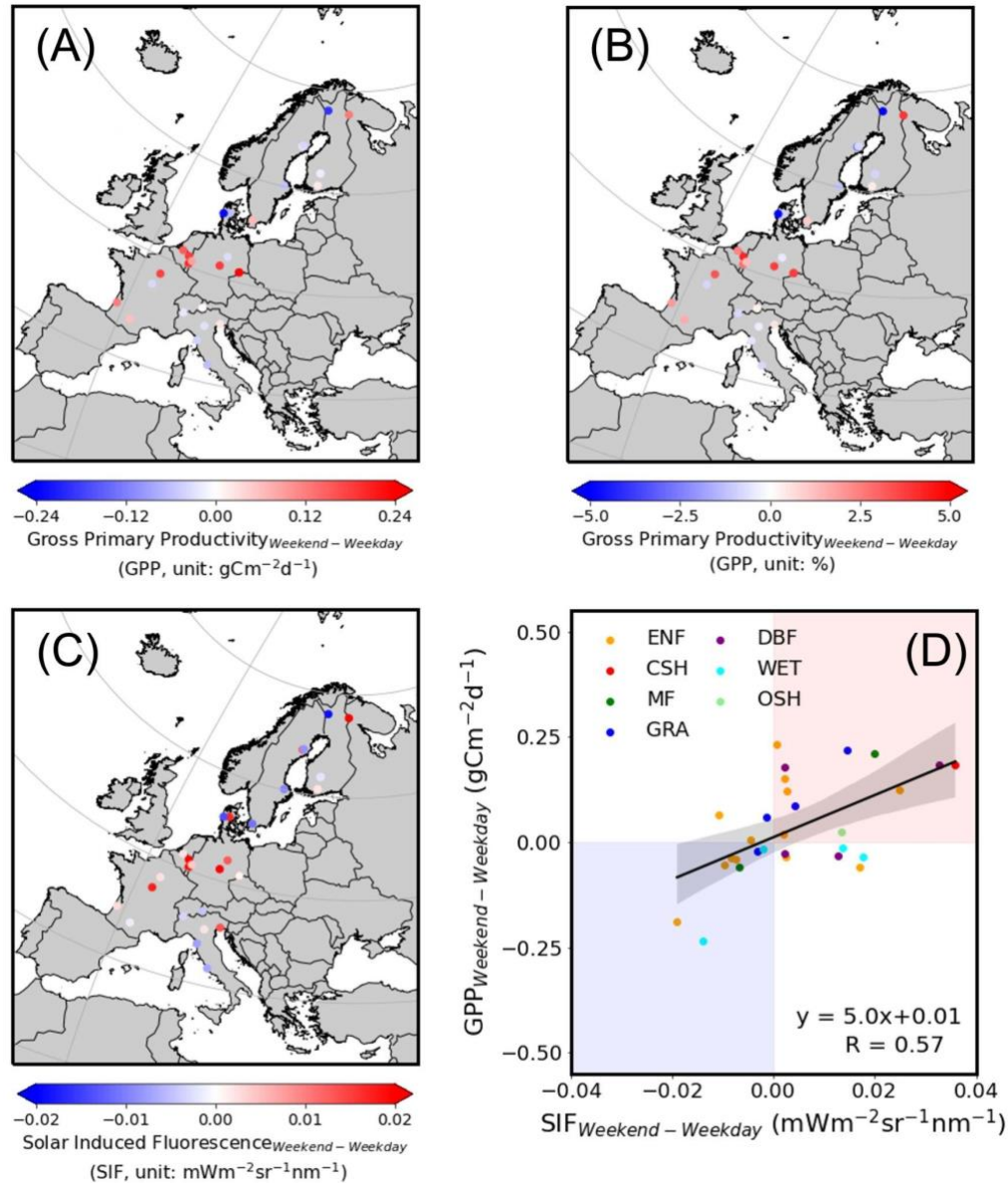
Supplementary Figure 10. The estimated standard error of the Sensitivity of solar induced fluorescence to aerosols corresponding to Figure 3. The standard error is calculated through regression coefficient analysis using the “statsmodels” package in Python.



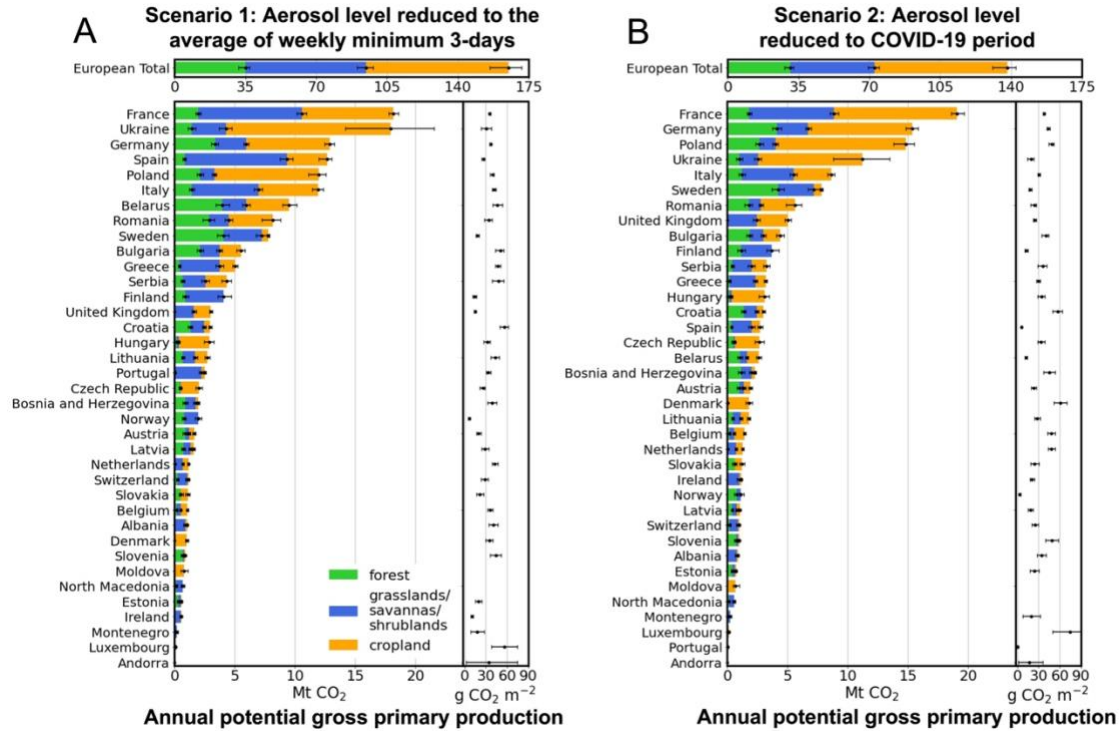
Supplementary Figure 11. Relative changes of TROPOMI solar induced fluorescence (unit: %) responding to 0.1 increase in aerosol optical depth in Europe derived from weekly patterns, which refers to weekend minus weekday signals, during 2018, 2019 and 2021. The grids marked with black dots indicate that the regression coefficient is significant with p -value < 0.05. The histogram shows the distribution of the derived sensitivity and the black dashed line represent the median. The results correspond to those shown in **Figure 3**, with normalized by the 95th percentile of daily solar induced fluorescence in each pixel and 0.1 scaling of aerosol optical depth.



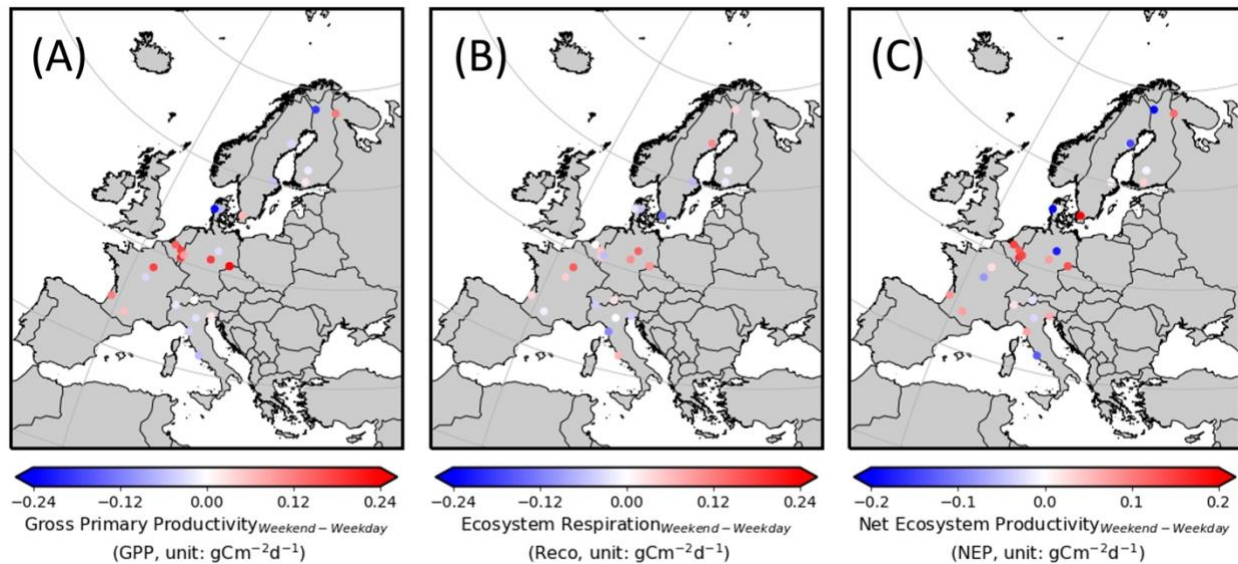
Supplementary Figure 12. The correlation between daily TROPOMI solar-induced fluorescence (SIF) and eddy covariance gross primary productivity (GPP) for days when both measurements are available. The titles give the site name and corresponding land cover defined in Supplementary Table S1.



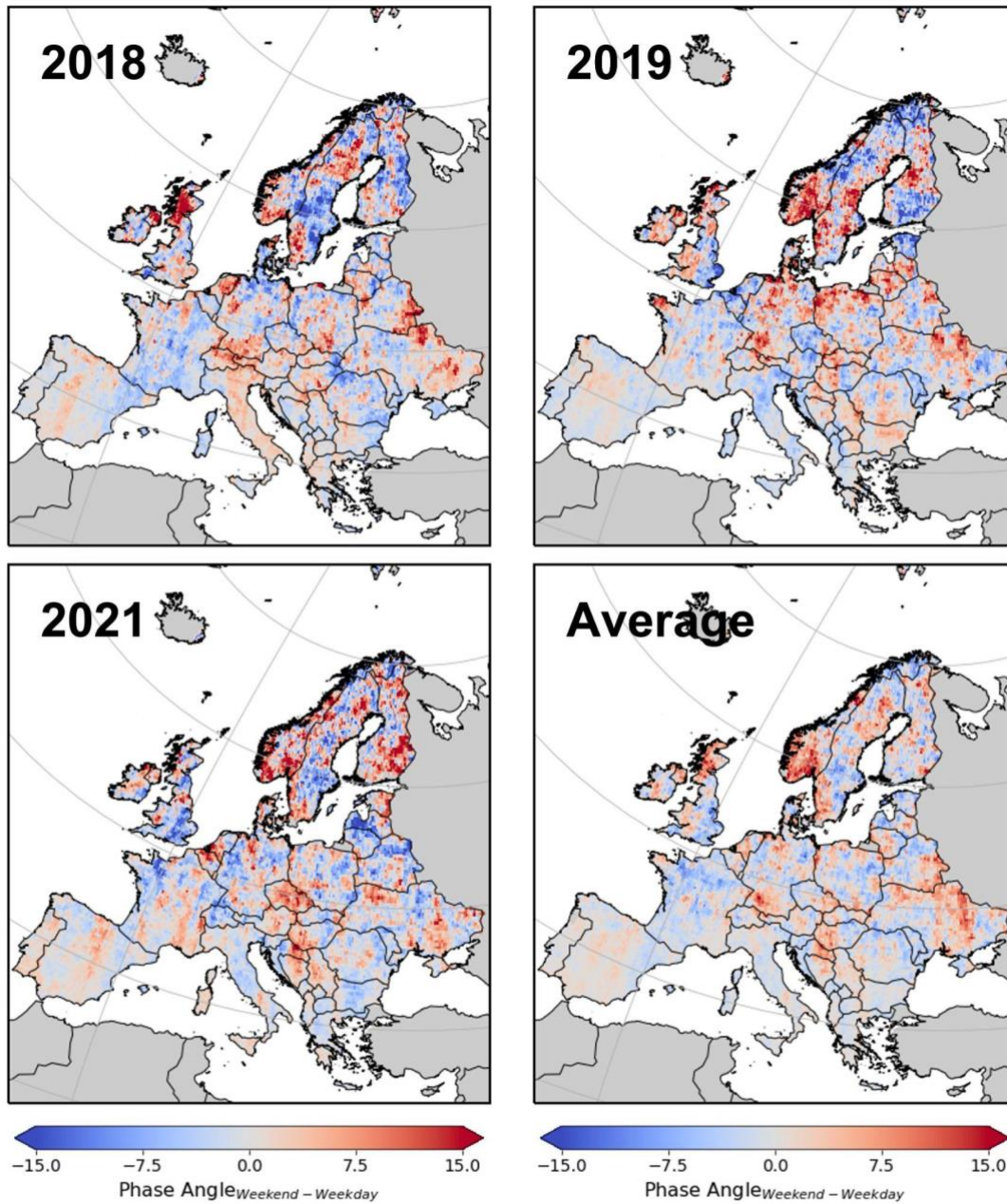
Supplementary Figure 13. The averaged difference between weekend and weekday measurements of (A) gross primary productivity estimated from eddy covariance measurements, (B) percent changes in gross primary productivity estimated from eddy covariance measurements, (C) TROPOMI solar-induced fluorescence at the 0.25-degree grid cell where the eddy covariance tower is located, and (D) the comparison between the two during 2018, 2019, and 2021. Only days with both measurements available are considered. Different colors in (D) represent different land cover types defined in **Supplementary Table S1**.



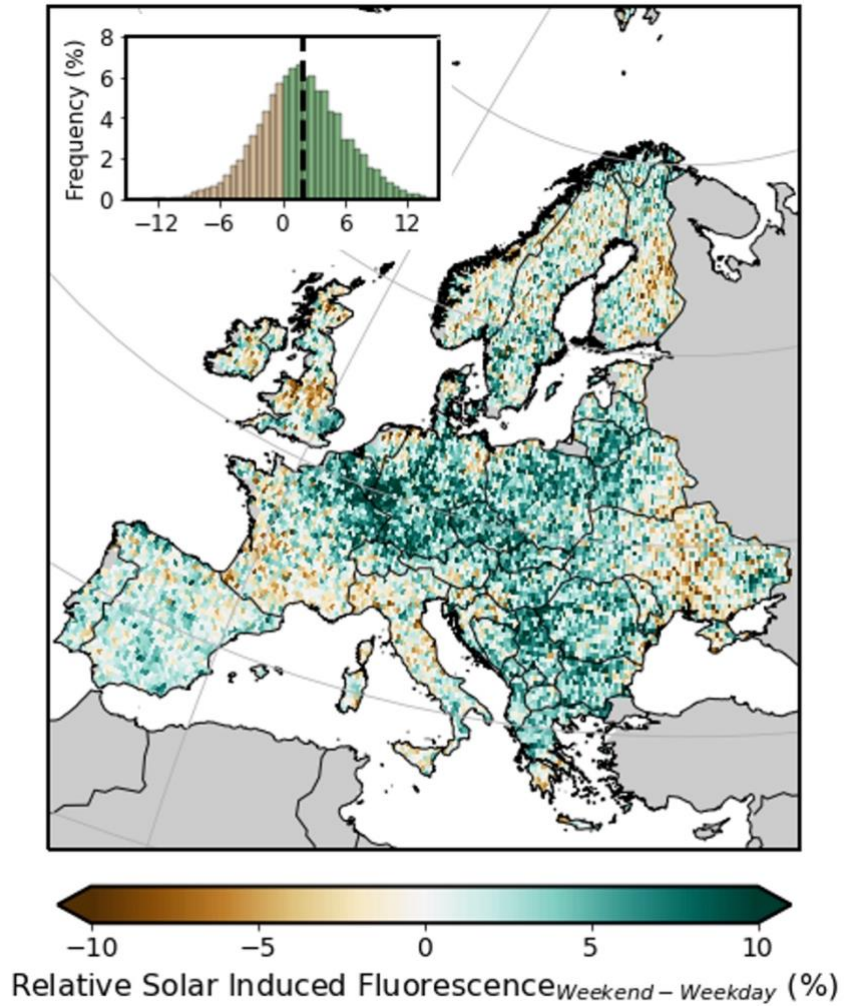
Supplementary Figure 14. Annual gross primary production increases through aerosol pollution reduction in two pollution mitigation scenarios. The increase in country-level annual net carbon uptake under pollution mitigation scenarios in Europe, with aerosol level reduced to (A) the average of weekly minimum 3-days and (B) COVID-19 period, represented by year 2020. Green, blue, and yellow bars represent the increase of annual carbon uptake by forest, grasslands/savannas/shrublands and cropland, respectively. To estimate the range of estimated values, we consider the uncertainties associated with SIF sensitivities to AOD, the conversion factor of SIF to GPP, the conversion factor of GPP to NEE, and the definition of the growing season based on the fraction of photosynthetically active radiation (fPAR). We employed a bootstrap approach, resampling the data 1000 times. The central estimates are represented by the median, while the upper and lower bounds correspond to the 95th and 5th percentiles, respectively.



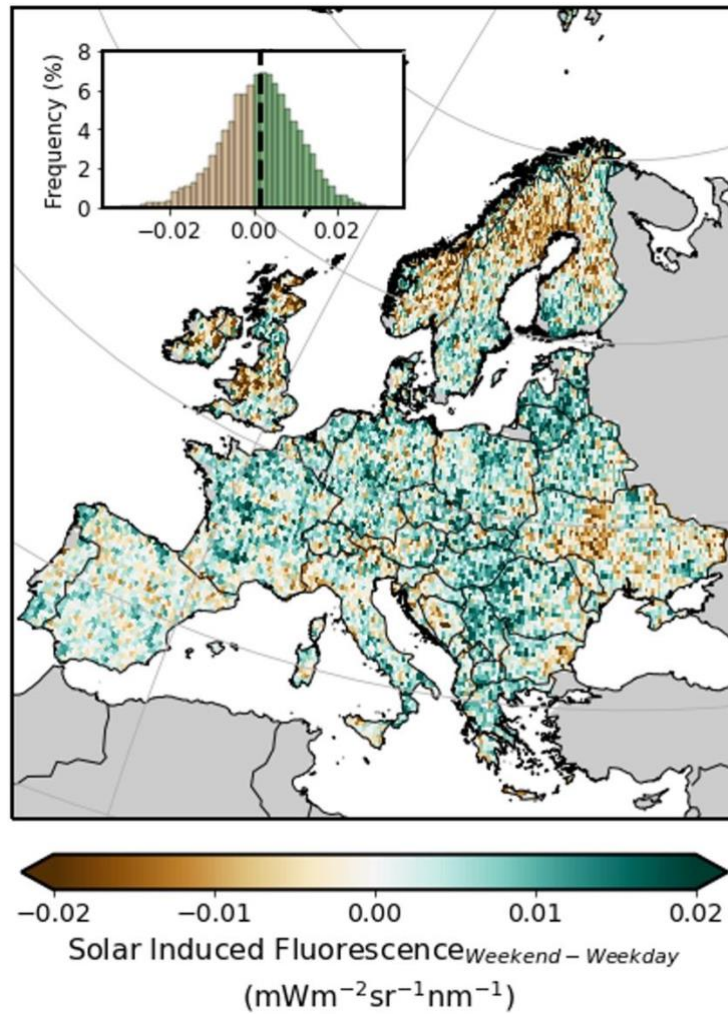
Supplementary Figure 15. The averaged difference between weekend and weekday measurements of (A) gross primary productivity, (B) ecosystem respiration and (C) net ecosystem productivity estimated from eddy covariance measurements during 2018, 2019, and 2021. Only days with both measurements available are considered.



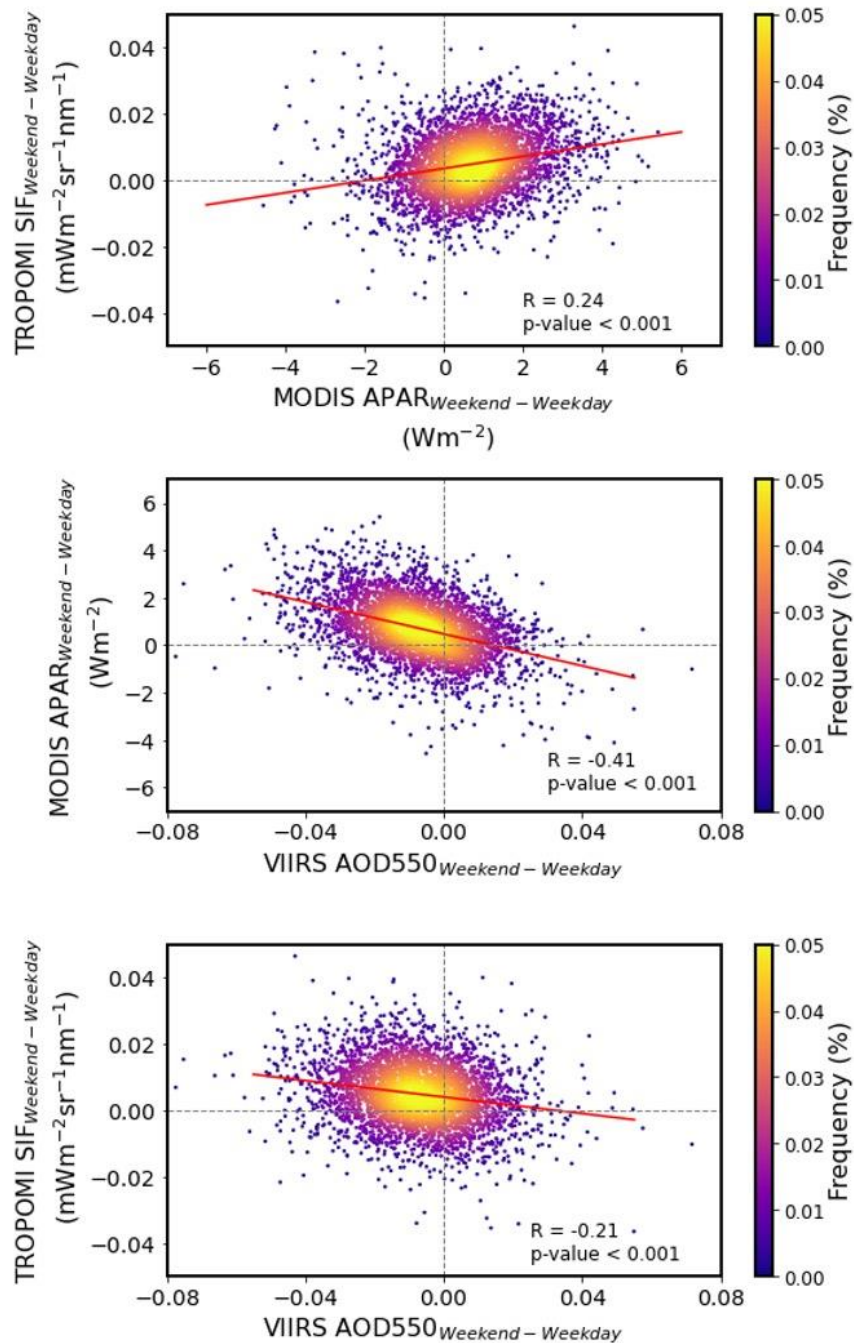
Supplementary Figure 17. The difference in TROPOMI phase angles between weekend and weekday in Europe during 2018, 2019, 2021 and the three-year averages.



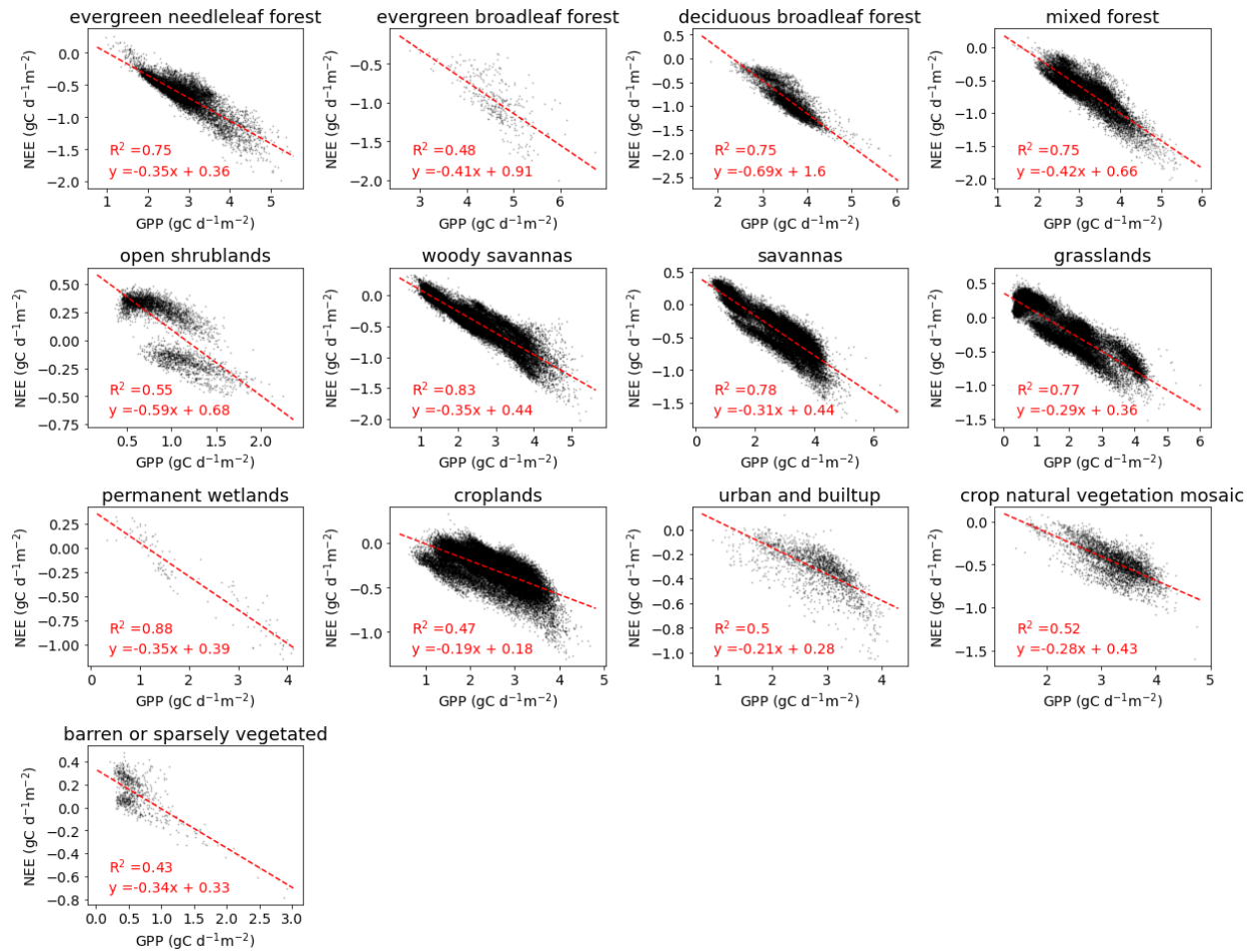
Supplementary Figure 18. Weekend minus weekday relative TROPOMI solar induced fluorescence in Europe during 2018, 2019 and 2021. The relative SIF represents SIF normalized by the continuum level NIR-reflected radiance. The spatial pattern is consistent with Figure 1, indicating that the widespread decrease in SIF is predominantly associated with reductions in absorbed photosynthetically active radiation (APAR), rather than being influenced by signal attenuation caused by aerosols. The insert histogram shows the distribution, and the dashed black line represents the median values.



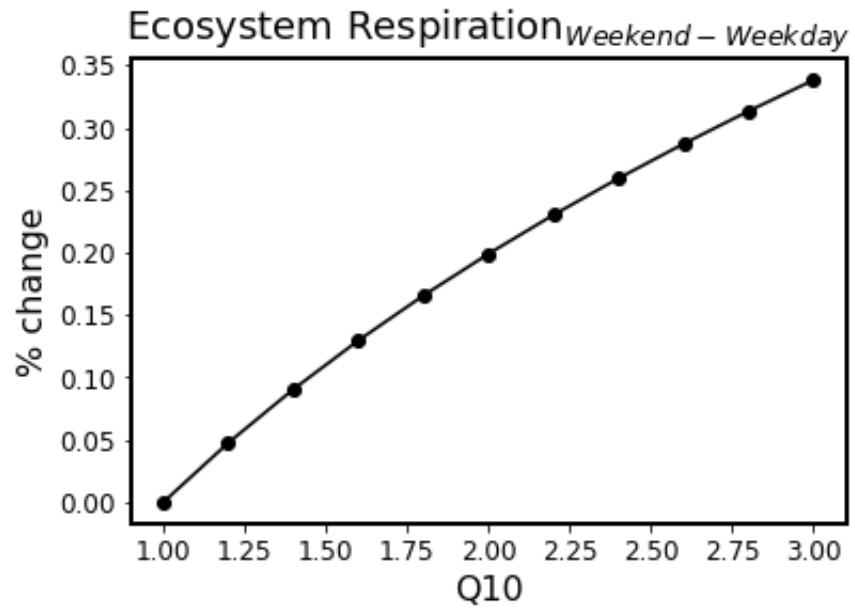
Supplementary Figure 19. Difference between weekend and weekday (2018, 2019 and 2021) of TROPOMI using the TROPOSIF product produced by Guanter et al. (1) The spatial pattern is consistent with the Caltech TROPOMI SIF by Köhler et al. (2) used in this study. The insert histogram shows the distribution, and the dashed black line represents the median values.



Supplementary Figure 20. The relationship among solar-induced fluorescence (SIF), absorbed photosynthetically active radiation (APAR), and aerosol optical depth at 550nm (AOD550). All available weekly difference data of SIF, APAR, and AOD observations from 2018 to 2021 (excluding 2020) are used here. The linear relationship observed between SIF and AOD suggests that the impact of AOD on SIF at ambient AOD levels can be adequately captured using a linear regression framework.



Supplementary Figure 21. FLUXCOM annual net ecosystem change (NEE) vs. gross primary productivity (GPP) for each land cover type in Europe. The study region is defined as in **Figure 1**. The spatial resolution of FLUXCOM is 0.083 degrees. The land cover map is based on MODIS IGBP classification. Deciduous needleleaf forest and closed shrubland are excluded due to their limited coverage in the study region. Snow and ice are also excluded in the analysis.



Supplementary Figure 22. Europe-averaged relative change in ecosystem respiration over the weekend compared to weekday with different Q10 values.

Supplementary Table S1. The location and IGBP land cover classification of eddy covariance sites used in the study. ENF, CSH, MF, GRA, DBF, WET, and OSH represents evergreen needleleaf forests, closed shrublands, mixed forests, grasslands, deciduous broadleaf forests, permanent wetlands and open shrublands, respectively.

Site	Lon	Lat	IGBP	Q10
BE-Bra	4.52	51.31	ENF	1.63
BE-Maa	5.63	50.98	CSH	1.77
BE-Vie	6.00	50.30	MF	1.86
CH-Dav	9.86	46.82	ENF	2.00
DE-Gri	13.51	50.95	GRA	1.81
DE-Hai	10.45	51.08	DBF	1.98
DE-HoH	11.22	52.09	DBF	2.32
DE-RuR	6.30	50.62	GRA	2.13
DE-Tha	13.57	50.96	ENF	1.89
DK-Gds	9.33	56.07	ENF	1.15
DK-Skj	8.40	55.91	WET	2.15
FI-Hyy	24.29	61.85	ENF	2.02
FI-Ken	24.24	67.99	ENF	2.41
FI-Let	23.96	60.64	ENF	2.32
FI-Sii	24.19	61.83	WET	2.26
FI-Var	29.61	67.75	ENF	1.97
FR-Bil	-0.96	44.49	ENF	1.94
FR-Fon	2.78	48.48	DBF	1.81
FR-LGt	2.28	47.32	WET	2.16
FR-Tou	1.37	43.57	GRA	1.09
IT-BFt	10.74	45.20	DBF	1.45
IT-Cp2	12.36	41.70	MF	0.99
IT-Lsn	12.75	45.74	OSH	1.95
IT-SR2	10.29	43.73	ENF	1.64
IT-Tor	7.58	45.84	GRA	2.96
SE-Deg	19.56	64.18	WET	2.57
SE-Htm	13.42	56.10	ENF	2.55
SE-Nor	17.48	60.09	ENF	2.04
SE-Svb	19.77	64.26	ENF	2.26

Supplementary Table S2. The regression coefficient and associated standard error corresponding to Supplementary Figure 21. The regression model used is as follows:

$$NEE = \beta_{NEE-GPP} \times GPP + \beta_0$$

where NEE represents the net ecosystem exchange and GPP represents gross primary productivity.

IGBP	$\beta_{NEE-GPP}$	standard error of $\beta_{NEE-GPP}$	β_0	standard error of β_0
evergreen needleleaf forest	-0.353	0.002	0.355	0.006
evergreen broadleaf forest	-0.410	0.023	0.909	0.108
deciduous broadleaf forest	-0.691	0.005	1.603	0.019
mixed forest	-0.417	0.002	0.664	0.007
open shrublands	-0.587	0.008	0.679	0.008
woody savannas	-0.349	0.001	0.438	0.003
savannas	-0.305	0.001	0.442	0.003
grasslands	-0.286	0.001	0.356	0.002
permanent wetlands	-0.346	0.012	0.393	0.029
croplands	-0.190	0.001	0.182	0.003
urban and builtup	-0.214	0.005	0.278	0.014
crop natural vegetation mosaic	-0.278	0.004	0.428	0.014
barren or sparsely vegetated	-0.343	0.014	0.331	0.010

References

1. L. Guanter, *et al.*, The TROPOSIF global sun-induced fluorescence dataset from the Sentinel-5P TROPOMI mission. *Earth Syst Sci Data* **13**, 5423–5440 (2021).
2. P. Köhler, *et al.*, Global retrievals of solar-induced chlorophyll fluorescence with TROPOMI: First results and intersensor comparison to OCO-2. *Geophys Res Lett* **45**, 10–456 (2018).